Journal of Neurochemistry, 2006, **99**, 426–437 doi:10.1111/j.1471-4159.2006.03967.x

Selective blockage of $K_v1.3$ and $K_v3.1$ channels increases neural progenitor cell proliferation

Stefan Liebau,* Christian Pröpper,* Tobias Böckers,* Frank Lehmann-Horn,† Alexander Storch,‡ Stephan Grissmer† and Oliver H. Wittekindt†,§

*Department of Anatomy and Cell Biology and †Department of Applied Physiology, University of Ulm, Ulm, Germany

‡Department of Neurology, Technical University of Dresden, Dresden, Germany

§Department of General Physiology, University of Ulm, Ulm, Germany

Abstract

The modulation of cell proliferation in neural progenitor cells (NPCs) is believed to play a role in neuronal regeneration. Recent studies showed that K^+ channel activity influenced cell proliferation. Therefore, we examined NPCs for K^+ channels and tested whether NPC self renewing can be modulated by synthetic K^+ channel modulators. The whole-cell K^+ current was partly K^+ dependent and showed a cumulative inactivating component. Two tetra-ethyl-ammonium ion (TEA)-sensitive K^+ currents with different voltage dependencies (IC_{50}^1 = 65 μM, $E_{50} = -0.3 \pm 1.3$ mV and $IC_{50}^2 = 8$ mM, $E_{50} = -15.2 \pm 2.8$ mV) and an almost TEA-insensitive current were identified. Kaliotoxin blocked approximately 50% of the entire K^+ currents ($IC_{50} = 0.25$ nM). These properties resembled functional characteristics of $K_v1.4$, $K_v1.3$ and $K_v3.1$ channels. Transcripts for these channels, as well as proteins for $K_v1.3$ and $K_v3.1$, were identified. Immunocytochemical staining revealed $K_v1.3$ and $K_v3.1$ K^+ channel expression in almost all NPCs. The blockage of $K_v3.1$ by low concentrations of TEA, as well as the blockage of $K_v1.3$ by Psora-4, increased NPC proliferation. These findings underline the regulatory role of K^+ channels on the cell cycle and imply that K^+ channel modulators might be used therapeutically to activate endogenous NPCs.

Keywords: neural progenitor, potassium channels, proliferation.

J. Neurochem. (2006) **99**, 426–437.

Recent studies investigated the expression of ion channels in different populations of neuronal and glial precursor cells. *Shaker*-like potassium channels of the K_v1 type were observed for oligodendrocyte precursor cells (Schmidt *et al*. 1999; Vautier *et al*. 2004). Neuronal progenitor cells from the subventricular zone and the rostral migration stream are found to express Ca^{2+}-dependent and tetra-ethyl-ammonium ion (TEA)-sensitive delayed rectifying K^+ currents (Wang *et al*. 2003). Similar K^+ currents are also described for differentiating human neural progenitor cells (NPCs; Hermann *et al*. 2004a). This heterogeneity in the expression of K^+ currents can be explained by the different investigated cell types. It is commonly accepted that cell differentiation and maturation affects the expression pattern of ion channels and therefore the electrophysiological properties of the cell membrane. These changes of the functional properties of ion currents during cell maturation were described for immortalized neural progenitor cells (Herberth *et al*. 2002) as well as for developing neurons (Ribera 1999; Spitzer *et al*. 2000).

Recent studies support the hypothesis that cell proliferation can be regulated by modulation of K^+ channel activity. Division of pancreatic tumour cells was repressed by selective blockage of K^+ channels of the IK-type (Jager *et al*. 2004). The inhibition of the *Shaker*-like K^+ channel $K_v1.3$ down-regulated mitosis of chronically activated T-lymphocytes (Beeton *et al*. 2001, 2005). Additionally, K^+ channels were also reported as molecular determinants in

Received October 11, 2005; revised manuscript received April 11, 2006; accepted April 19, 2006.

Address correspondence and reprint requests to Dr Oliver H. Wittekindt, Department of General Physiology, Albert-Einstein-Allee 11, 89081 Ulm, Germany. E-mail: Oliver.Wittekindt@uni-ulm.de

Abbreviations used: BrDU, 5′-bromo-2′-deoxy-uridine; DAPI, 4,6-diamidino-2-phenylindole; EGF, epidermal growth factor; HMBS, hydroxymethylbilane synthase; K-sol, potassium solution; KTX, kaliotoxin; NPC, neural progenitor cell; N-sol, normal solution; PBS, phosphate-buffered saline; TEA, tetra-ethyl-ammonium ions; TMA, tetra-methyl-ammonium ions.

lineage progression of oligodendrocyte precursor cells (Gallo *et al*. 1996; Attali *et al*. 1997; Knutson *et al*. 1997; Vautier *et al*. 2004).

We focused our investigations on a possible key role of K^+ channels for triggering progeny of murine mesencephalic NPCs. Cells, which were used for the present investigation were long-term cultured under-non-differentiating conditions (Storch *et al*. 2001). Long-term cultured NPCs provide a source of homogenous cell populations of progenitor cells and allow the investigation of NPCs during early stages of differentiation.

The functional expression of K^+ channels was studied by the whole-cell patch-clamp technique in parallel with immunocytochemical, as well as molecular biological methods. The effect of the identified K^+ channels on NPC proliferation was examined by the selective K^+ channel blockage during the culturing of NPCs. Our data showed that the selective blockage of K^+ channels increases NPC proliferation *in vitro*.

Materials and methods

Expansion of mesencephalic NPCs

Adult pregnant Sprague–Dawley rats were anaesthetized and killed with 100% CO_2, embryos (embryonic stage E14.5) were removed from the uterus and placed into ice-cold Hank's balanced salt solution (HBSS) supplemented with 1% penicillin/streptomycin and 1% glucose (all from Gibco, Tulsa, OK, USA). Their brains were removed and the midbrain was then aseptically prepared. The meninges were carefully removed from the tissue after preparation of the midbrain area. For expansion of neurospheres, tissue samples were incubated in 0.1% trypsin (Sigma, St Louis, MO, USA) for 10 min at room temperature (21–23°C), incubated in Dnase I (40 mg/mL; Sigma) for 10 min at 37°C, and homogenized to a quasi-single-cell suspension by gentle triturating. The cells were added to 25-cm^2 flasks ($2 \times 3\ 10^6$ viable cells per flask) in serum-free medium containing 63% Dulbecco's modified Eagle's medium (DMEM) high glucose, 32% Ham's F12, 1% glutamate, 2% B27 supplement, 1% penicillin/streptomycin and 1%-non-essential amino acids (all from Gibco), supplemented with 20 ng/mL of the mitogen epidermal growth factor (EGF; Sigma). Cultures were placed in a humidified incubator at 37°C and 5% CO_2, 95% air (21% O_2). After 4–7 days, sphere formation was observed. The medium was changed once a week while growth factor was added twice a week. The neurospheres were expanded for an additional 3 weeks (in total 3–5 passages) in suspension before adherent proliferation was initiated by plating the cells (about 20 000 cells/well) with the same media, supplemented with 5% serum replacement (Gibco) onto poly-L-lysine-coated glass cover slips in 24-well plates. All the following studies were then performed 1–24 h after transferring the cells to the well-plates.

Electrophysiological experiments

Neurospheres were transferred onto a poly-L-lysine-coated glass coverslip and were kept under culturing conditions for 1 to 4 h before electrophysiological investigation. The coverslips were placed into a perfusion chamber directly before measurement and were permanently superfused with normal solution (N-sol, in mM: NaCl 160, KCl 4.5, $CaCl_2$ 2, $MgCl_2$ 1, HEPES 5, pH 7.4), potassium solution (K-sol, in mM: KCl 164.5, $CaCl_2$ 2, $MgCl_2$ 1, HEPES 5, pH 7.4) and K0-solution (K0-sol, in mM: NaCl 164.5, $CaCl_2$ 2, $MgCl_2$ 1, HEPES 5, pH 7.4). Only those cells were taken for electrophysiological investigations, which started to migrate from the attached neurosphere. Pipettes were pulled in three stages with a tip resistance ranging from 1.5 to 2.5 MΩ when filled with pipette solution (KF-sol, in mM: KF 145, EGTA 10, HEPES 10, $MgCl_2$ 1, pH 7.2). A HEKA EPC9 amplifier (HEKA Elektronik, Lambrecht, Germany) was used with Pulse and PulseFit (HEKA Elektronik) as data acquisition and analysis software.

The membrane potential was stepped from −80 mV to +40 mV for 200 ms and kept at −80 mV for 30 s between voltage steps for investigating the effect of kaliotoxin (KTX; Bachem, Weil am Rhein, Germany). Psora-4 (kindly provided by Professor Hänsel, University of Kiel, Germany) was tested in the presence of 1 mM TEA and using voltage steps as described, but with a duration of 500 ms. Peak currents at a certain Psora-4 concentration were measured when they reached a steady state. This was achieved after at least 12 voltage steps at a certain Psora-4 concentration. Curve fitting was carried out using IgorPro 3.12 (Wavemetrics, Portland, OR, USA) as described (Motulsky and Christopoulos 2004). The calculated ± value reflects the uncertainty of the fit.

Cumulative inactivation was tested by applying 10 repetitive voltage steps from −80 mV to +40 mV with a duration of 200 ms. The membrane potential was clamped to −80 mV for 1 s. Time constants were calculated as best fit through the data points according to a double exponential equation using IgorPro 3.12 (Wavemetrics).

Semi-quantitative real-time one-step RT-PCR

Semi-quantitative real-time one-step RT-PCR was carried out using the LightCycler System (Roche, Mannheim, Germany), and amplification was monitored and analysed by measuring the binding of the fluorescence dye SYBR Green I to double-stranded DNA. One microlitre of total RNA was reversely transcribed and subsequently amplified using QuantiTect SYBR Green RT-PCR Master mix (Qiagen, Valencia, CA, USA) and 0.5 μmol/L of both sense and antisense primers. Tenfold dilutions of total RNA were used as external standards. Internal standards and samples were simultaneously amplified. After amplification, melting curves of the RT-PCR products were acquired to demonstrate product specificity. Results are expressed relative to the housekeeping gene hydroxymethylbilane synthase (HMBS). Primer sequences, lengths of the amplified products and melting analyses are summarized in Fig. 1.

Western blotting

Whole-cell protein extracts were denatured after sonication at 75°C for 2 min in order to avoid oligomerization of channel proteins. The proteins were separated by standard sodium dodecyl sulfate – polyacrylamide electrophoresis gel (SDS–PAGE) with 8% total monomer concentration and were electro blotted by standard protocols onto nitrocellulose membranes. Specific primary antibodies were: anti-K_v1.3 diluted 1 : 400, anti-K_v1.4 diluted 1 : 400 (Alomone Laboratories, Jerusalem, Israel) and anti-K_v3.1 diluted

Channel (gene name)	Primer sequence	Product length (bp)	Melting curve
$K_V1.1$ (Kcna1)	5′-GGCAACCCGAAGAAACGC-3′ 5′-GCCTCCTCGCCAACTC-3′	188	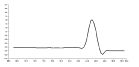
$K_V1.2$ (Kcna2)	5′-CCTATGACCCAGAGGCAGAC-3′ 5′-CATCCGTTTCTTGGGGTCTC-3′	134	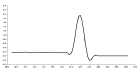
$K_V1.3$ (Kcna3)	5′-GCTGGTGCGATTCTTTGC-3′ 5′-CATAGCCTGCTGCCCATTAC-3′	145	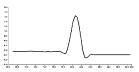
$K_V1.4$ (Kcna4)	5′-CGGTGGAAGGCACTGGAG-3′ 5′-CTCAGTTCGCTGTCGCCTC-3′	125	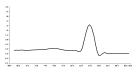
$K_V1.5$ (Kcna5)	5′-CCAGCAAGGCAGGGTTCTC-3′ 5′-CGGATGACTCGGAGGATGG-3′	169	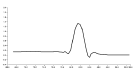
$K_V3.1$ (Kcnc1)	5′-CGAGCTGGAGATGACCAAGAG-3′ 5′-AGAAGAGGGAGGCAAAGGC-3′	155	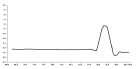
$K_V3.2$ (Kcnc2)	Rn_Kcnc2_1_SG QuantiTect Primer Assay QT00184807 (Qiagen, Germany)	77	Not amplified
$K_V3.3$ (Kcnc3)	5′-GCGGCGACAGCGGTAAG-3′ 5′-GGTCAAAGAAGAACTCGTCC-3′	165	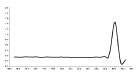
HMBS	5′-CGACACTGTGGTAGCGATGC-3′ 5′-CCTTGGTAAACAGGCTCTTCTCTC-3′	134	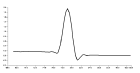

Fig. 1 Primer sequences and melting curve analysis of semiquantitative real-time RT-PCR experiments. Names of gene products and gene names, primer sequences and product length are given. The melting curves are plotted as dF(T)/dT (*y*-axis) against T [°C] (*x*-axis).

1 : 400 (Chemicon, Temecula, CA, USA). Pre-adsorption controls with the specific antigen supplied with the antibodies were carried out as negative controls according to the manufacturer's protocol. The enhanced chemiluminescence (ECL) detection kit (Amersham Pharmacia, Freiburg, Germany) was used for immune detection according to the manufacturer's protocol.

Immunocytochemical detection

For immunofluorescence detection of K^+ channel subunits, cultured cells were fixed with 4% paraformaldehyde (PFA)/1.5% sucrose/phosphate-buffered saline (PBS) for 20 min at room temperature. After washing three times with 1 × PBS for 5 min at room temperature, the cells were permeabilized for 5 min on ice in a buffer containing 0.2% Triton-X-100/0.1% Na-Citrate/PBS and washed again three times with 1 × PBS. Blocking was performed with 10% FCS/PBS for 1 h at room temperature followed by incubation with the primary antibodies, diluted in PBS, for 3 h. After a further washing step, the cells were incubated with the secondary antibody conjugates for 90 min at room temperature, washed three times with 1 × PBS and then with aqua bidest for 3 min and mounted in Mowiol (Sigma). Cell nuclei were counter stained with 4,6-diamidino-2-phenylindole (DAPI). The following primary antibodies were used: rabbit anti-Kv1.3 diluted 1 : 200, rabbit anti-Kv1.4 diluted 1 : 50, rabbit anti-Kv3.1 diluted 1 : 200 (all from Alomone Laboratories) and mouse anti-nestin monoclonal diluted 1 : 500 (BD Biosciences, Bedford, MA, USA); fluorescence-labelled secondary antibodies were Alexa Fluor® 555 (red, used filter set: excitation BP 534–558 nm, FT 560, emission BP 575–640 nm) and Alexa Fluor® 488 (green, used filter set: excitation BP 450–490 nm, FT 510, emission BP 515–565 nm) (Invitrogen, Karlsruhe, Germany), both diluted 1 : 500. Images were captured using an upright fluorescence microscope (Axioskop 2, Zeiss, Oberkochen, Germany) equipped with a Zeiss CCD camera (16 bits; 1280 × 1024 pixels per image), and analysed using Axiovision software (Zeiss).

Cryosections

Neurospheres were high-pressure frozen, freeze substituted and embedded in London Resin (LR-gold, Polysciences, Eppelheim, Germany), a special hydrophilic resin used for embedding of tissue

in the immunocytochemistry at electron microscopy level, as described (Walther and Ziegler 2002) with some modifications: The substitution medium consisted of acetone with 0.5% of uranyl acetate and 5% of water. As embedding medium LR-gold was used, polymerization was carried out at −18°C. Samples were semi-thin sectioned (thickness 2 μm). $K_v1.3$, $K_v3.1$ antibodies (1 : 10 diluted) and were used in immunocytochemical staining. Secondary detection was carried out as described above.

Proliferation assay

For identifying currently dividing cells, the bromo-2′-deoxy-uridine labelling and detection kit (Roche) was used. Dividing cells incorporate 5′-bromo-2′-deoxy-uridine (BrDU) into replicating DNA in place of thymidine. Incorporated BrDU can be detected via immunocytochemical labelling following the developer's manual. Cell nuclei representing total number of cells were DAPI counter stained. Ratios of BrDU-positive cells were generated according to N_{BrDU+}/N_{DAPI} (N_{BrDU+} = number of BrDU positive cells, N_{DAPI} = total number of cells).

Results

The whole-cell mode of the patch-clamp technique was used to investigate whole-cell currents of long-term cultured mesencephalic NPCs. The membrane potential was stepped to −120 mV for 50 ms followed by a 200-ms voltage ramp from −120 mV to +40 mV and was clamped to −80 mV for 10 s between voltage ramps. In N-sol as bath solution, we observed outward ramp currents at membrane potentials above −20 mV (Fig. 2). The outward current clearly showed two humps, indicating at least two different types of voltage-activated currents. Changing the bath solution to K-sol resulted in a change of the current as predicted from the opening of voltage-gated K^+ channels which conduct inward current below and outward current above 0 mV.

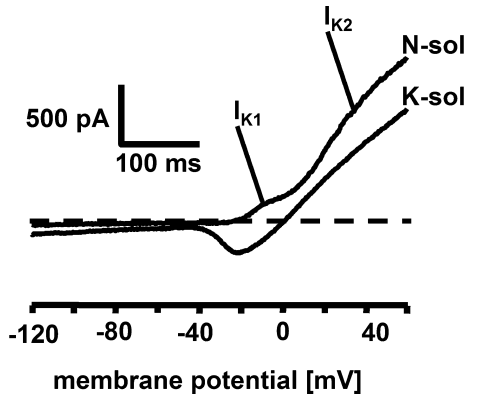

Fig. 2 Whole-cell ramp currents of neural progenitor cells. The membrane potential was clamped to −120 mV for 50 ms followed by a 400 ms voltage ramp from −120 mV to +60 mV. Representative whole-cell ramp currents of NPCs are shown. Bath solutions are given on the right. I_{K1} and I_{K2} assign the humps, which were caused by two types of outward current.

When the membrane potential was stepped from −80 mV to +40 mV for 200 ms, as can be seen in Fig. 3, the K^+ current showed a time-dependent decay during depolarization. This current decay can be fitted by two exponentials according to $I = I_0 + (I_{max}–I_0)a_0 \times \exp(t/\tau_{slow}) + (I_{max}–I_0)(1–a_0)\exp(t/\tau_{fast})$ with I_0 as a non-inactivating current component, I_{max} as the maximum current, a_0 as the fraction of inactivating K^+ current carried by the slow inactivating current, τ_{slow} and τ_{fast} as time constants of inactivation for the slow and fast inactivating K^+ currents. The fraction of inactivating K^+ current, which was carried by the slow inactivating current component was found to be 0.6 ± 0.08. The slow inactivating current decayed with a time constant of τ_{slow} = 167 ± 13 ms. The fast inactivating current showed a

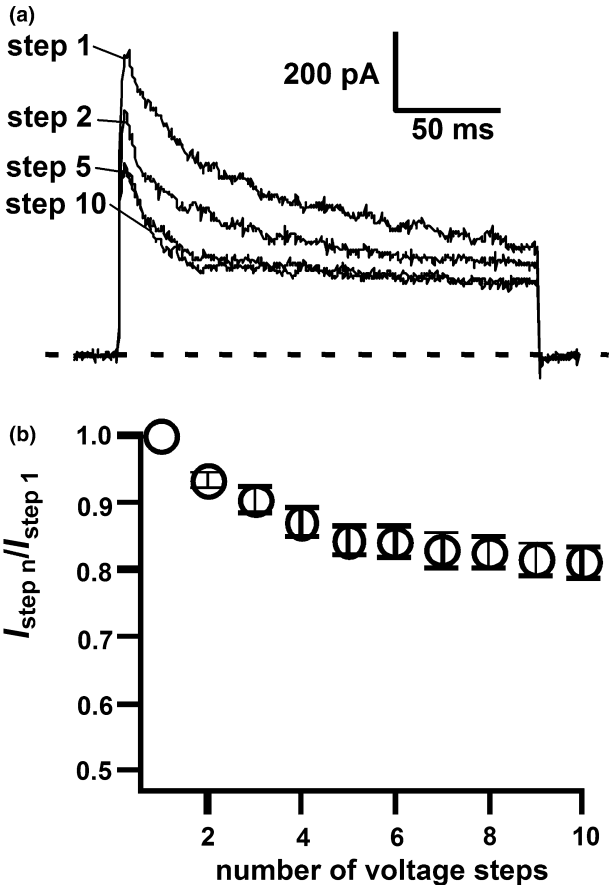

Fig. 3 Cumulative inactivation of whole-cell currents of neural progenitor cells. Ten repetitive 200-ms voltage steps from −80 mV to +40 mV were applied with a 1-s interval between each depolarizing step. N-sol was used as bath solution. (a) Representative outward currents are shown. For better clarity, only outward currents for the 1st, 2nd, 5th and 10th voltage step (assigned as step 1, step 2, step 5 and step 10) are shown. (b) Relative peak currents were calculated according to $I/I_{step\ 1}$ with I as peak currents at any voltage step and $I_{step\ 1}$ as the peak current at the first voltage step and plotted as mean values ± SEM (n = 17) against the number of the voltage step.

time constant of $\tau_{fast} = 22 \pm 3$ ms (all values are mean values ± SEM, $n = 17$). Ten repetitive voltage steps from −80 to +40 mV with a 1-s interval led to a cumulative inactivation of K^+ current (Fig. 3b). The remaining relative peak current was calculated according to I_{step10}/I_{step1} with I_{step10} and I_{step1} as the peak currents elicited by the 10th and the first depolarization step, and was found to be 0.8 ± 0.02 (mean ± SEM, $n = 17$). Again, the time-dependent decay of the remaining inactivating current could be calculated by the double exponential fit described above. The fraction of the slow inactivating current decreased in these experiments to $a_0 = 0.4 \pm 0.1$. This indicates that the cumulative inactivation is predominantly caused by a decrease of slow inactivating current component. The extracellular depletion of K^+ from the bath solution abolished the fast inactivating K^+ current. The remaining relative peak current after K^+ depletion was found to be 0.47 ± 0.06 (mean ± SEM, $n = 5$). This indicates that this current is carried by K^+-dependent K^+ channels.

TEA blocked currents in NPCs in a concentration-dependent manner (Fig. 4). The relative peak currents in the presence of different TEA concentrations were plotted against the logarithm of TEA concentrations (Fig. 4b). The concentration–response curve was calculated as the best fit through the data points according to $I/I_{max} = a_0 + a_1 \times (1–a_0)/1 + 10\text{^}[\log(TEA) - \log IC_{50}^1] \times h + (1–a_1) \times (1–a_0)/1 + 10\text{^}\{[\log(TEA) - \log IC_{50}^2] \times h\}$ with a_0 as the remaining current, a_1 as fraction of the TEA sensitive relative currents, h as the Hill coefficient, which was fixed to 1 and $\log IC_{50}^1$ and $\log IC_{50}^2$ as the logarithm of the two IC_{50}s. Altogether, this curve indicated three K^+ channel populations. One population was found to be highly TEA-sensitive ($\log IC_{50}^1 = -4.2 \pm 0.07$) with an $IC_{50}^1 = 65$ μM, a second one with an intermediate TEA sensitivity ($\log IC_{50}^2 = -2.1 \pm 0.2$) with an $IC_{50}^2 = 8$ mM and an almost TEA-insensitive one as a third channel population (Table 1). The values a_0 and a_1 were calculated to be $a_0 = 0.15 \pm 0.02$ and $a_1 = 0.65 \pm 0.03$.

Since TEA was able to distinguish three types of K^+ currents in NPCs, we used 1 mM TEA in the bath solution to investigate the voltage dependence of different K^+ currents. Therefore, whole-cell currents were measured in N-sol and N-sol with 1 mM TEA. The remaining currents in the presence of TEA reflected the intermediate sensitive and insensitive component. Relative peak currents were calculated according to $g/g_{60\ mV}$, with g as peak conductance at any membrane potential and $g_{60\ mV}$ as peak conductance at +60 mV, and were plotted against the membrane potentials (Fig. 5). Curves through the data points were calculated according to the Boltzman equation $g/g_{60\ mV} = 1/[1 + \exp–(E\text{-}E_{1/2}/k)]$ with $E_{1/2}$ as the half maximal activating membrane potential and k as the steepness factor. The intermediate TEA-sensitive and TEA-insensitive current components were found to be activated at more negative membrane potentials ($E_{1/2} = -15.2 \pm 2.8$ mV, $k = 10.4 \pm 2.4$ mV). The highly TEA-sensitive currents were calculated as the difference of currents measured in N-sol in the absence and presence of TEA. This current component was found to lack any time-dependent inactivation during the depolarization step and to be activated at more positive membrane potentials according to the given Boltzman equation. ($E_{1/2} = -0.3 \pm 1.3$ mV, $k = 9.9 \pm 1.1$ mV). The relative peak conductance obtained in experiments with N-sol without any TEA as extracellular solution was also plotted against the

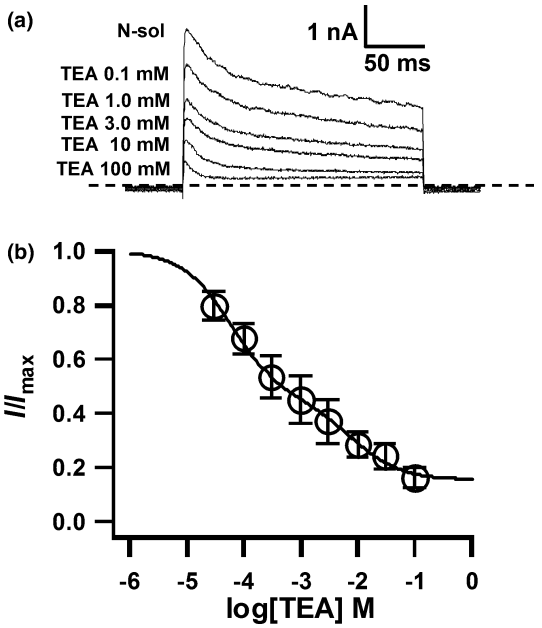

Fig. 4 Effect of TEA on current through voltage-dependent K^+ channels. N-sol was used as bath solution, in which Na^+ was replaced by TEA (final TEA concentrations: 30 μM, 100 μM, 300 μM, 1 mM, 3 mM, 10 mM, 30 mM and 100 mM). The membrane potential was stepped from −80 mV to +40 mV for 200 ms and kept for 30 s at −80 mV between voltage steps. (a) Representative whole-cell currents elicited by 200-ms voltage steps. For better clarity, current steps were only shown for N-sol as bath solution (N-sol) and for TEA concentrations as indicated. Peak currents were found to be 1.6 ± 0.4 nA (N-sol as bath solution, mean ± SEM, $n = 7$) and 0.3 ± 0.1 nA (100 mM TEA, mean ± SEM, $n = 5$). (b) TEA concentration–response curve. Relative peak currents were calculated according to I/I_{max} (I as currents with TEA, I_{max} as currents measured in N-sol) and were plotted as mean ± SEM (n between 5 and 7) against the logarithm of the TEA concentration. The concentration–response curve was calculated as the best fit through the data points according to $I/I_{max} = a_0 + a_1\text{*}(1–a_0)/1 + 10\text{^}[\log(TEA) - \log IC_{50}^1] \times h + (1–a_1)\text{*}(1–a_0)/1 + 10\text{^}\{[\log(TEA) - \log IC_{50}^2] \times h\}$ with a_0 as the remaining relative current, a_1 as fraction of the TEA-sensitive relative currents, h as the Hill coefficient, which was fixed to 1, and $\log IC_{50}^1$ and $\log IC_{50}^2$ as the logarithm of the two IC_{50}s. Best fit was obtained with $\log IC_{50}^1 = -4.2 \pm 0.07$ (corresponding to an $IC_{50}^1 = 65$ μM), $\log IC_{50}^2 = -2.1 \pm 0.2$ (corresponding to an $IC_{50}^2 = 8$ mM), $a_0 = 0.15 \pm 0.02$ and $a_1 = 0.65 \pm 0.03$.

Table 1 Biophysical (a) and pharmacological (b) properties of NPC whole-cell K^+ currents

(a)

Biophysical property	Observed values
Cumulative inactivation*	Yes
K^+ dependence	Yes
τ_{slow} (1st pulse/10th pulse)†	167 ± 13 ms/168 ± 34 ms
τ_{fast} (1st pulse/10th pulse)†	22 ± 4 ms/31 ± 4 ms
$E_{1/2}$ ($TEA_{high\ sensitive}$)	−0.3 ± 1.3 mV
$E_{1/2}$ ($TEA_{1\ mM}$)	−15.2 ± 2.8 mV

(b)

Pharmacological property	IC_{50} value observed	IC_{50} value reported for							
		$K_v1.1$	$K_v1.2$	$K_v1.3$	$K_v1.4$	$K_v1.5$	$K_v3.1$	$K_v3.2$	$K_v3.3$
TEA									
IC_{50}^1	65 μM	0.3 mM[a]	0.56 M[a]	10 mM[a]	> 0.1 M[c]	0.33 M[a]	0.2 mM[a]	63 μM[e]	140 μM[f]
IC_{50}^2	8 mM								
KTX	0.25 nM	41 nM[a]	> 1 μM[a]	650 pM[a]	Insen.[d]	> 1 μM[a]	> 1 μM[a]	ND	ND
Psora-4	0.5 nM	62 nM[b]	49 nM[b]	3 nM[b]	202 nM[b]	7.7 nM[b]	1.5 μM[b]	ND	ND

Values from the literature: [a](Grissmer *et al.* 1994); [b](Vennekamp *et al.* 2004); [c](Gomez-Hernandez *et al.* 1997); [d]Insen., insensitive (Legros *et al.* 2000); [e](Rettig *et al.* 1992); [f](Vega-Saenz *et al.* 1992). *Estimated from the peak current reduction elicited by repetitive 200-ms pulses from −80 mV to +40 mV every second; †calculated from currents, which were elicited by repetitive pulsing.

membrane potential. The curve through these data points were calculated as best fit according to a double Boltzman equation in which the above calculated $E_{1/2}$ and k-values were used, $g/g_{60\ mV} = a_0/[1 + \exp\text{-}(E + 0.3/9.9)] + 1\text{–}a_0/[1 + \exp\text{-}(E + 15.2/10.4)]$ and with a_0 as the fraction of the highly TEA-sensitive peak current, which was calculated to be 0.65 ± 0.09. This implies that 1 mM of TEA should block 65% of the entire peak currents and agrees with the observation that the remaining relative peak current at +60 mV in the presence of 1 mM TEA was 0.38 ± 0.1 (mean ± SEM, $n = 6$).

The effect of the $K_v1.3$-specific blocker KTX and the psoralene derivative Psora-4 onto whole-cell peak currents was tested in similar experiments (summarized in Table 1). KTX (Fig. 6) was applied to the bath up to concentrations of 30 nM and the concentration–response curve was calculated as best fit through the data points according to $I/I_{max} = a_0 + (1\text{–}a_0)/(1 + 10\text{^}(\log[KTX] - \log IC_{50}) \times h)$ with I/I_{max} as the relative peak current, a_0 as the relative KTX-insensitive peak current and h as Hill coefficient, which was fixed to $h = 1$. KTX was found to reduce whole-cell peak currents by approximately 50% ($a_0 = 0.5 \pm 0.005$, $n = 6$) with an IC_{50} value of 0.25 nM ($\log IC_{50} = -9.6 \pm 0.02$).

Psora-4 was tested in the presence of 1 mM TEA. It was applied to the bath solution up to concentrations of 10 nM (Fig. 7). The concentration–response curve was calculated according to the given equation $I/I_{1\ mM\ TEA} = a_0 + (1\text{–}a_0)/(1 + 10\text{^}(\log[Psora\text{-}4]\text{–}\log IC_{50}) \times h)$ with $I/I_{1\ mM\ TEA}$ as relative peak currents normalized to the peak current measured in the presence of 1 mM TEA,a_0 as the relative TEA and Psora-4 insensitive peak current and h as the Hill coefficient, which was fixed to $h = 1$. Psora-4 was found to reduce peak currents, which are insensitive to 1 mM TEA by 77% ($a_0 = 0.23 \pm 0.07$, $n = 6$) with an IC_{50} of 0.5 nM ($\log IC_{50} = -9.3 \pm 0.2$).

The results of the electrophysiological and pharmacological characterizations were summarized and compared with properties of those K^+ channels which share similarities to the K^+ channels we observed in NPCs. Taken together, we identified at least three different voltage-activated K^+ currents in NPCs. One current component was identified as a highly TEA-sensitive K^+ current, which was found to activate at more positive membrane potentials and did not show a time-dependent decay upon depolarization. A second current component was found to undergo a cumulative inactivation and a time-dependent decay upon depolarization ($\tau_{slow} = 167$ ms). A third component was observed as a fast inactivating current ($\tau_{fast} = 22$ ms), which did not undergo a cumulative inactivation. This current was found to be dependent on extracellular K^+. The fast and slow inactivating currents showed an intermediate sensitivity and insensitivity to TEA and activated at more negative membrane potentials. Furthermore, a prominent current component was found to be highly sensitive to KTX and Psora-4.

Identification of K^+ channel transcripts

Semiquantitative RT-PCR was performed on total RNA of undifferentiated NPCs in order to investigate the expression of those K^+ channels, which functionally resemble the properties of the observed K^+ currents. Therefore, only the expression of transcripts encoding for $K_v1.1$, $K_v1.2$, $K_v1.3$, $K_v1.4$, $K_v1.5$, $K_v3.1$, $K_v3.2$ and $K_v3.3$ were investigated. The highest RNA levels in NPCs were observed for $K_v1.3$, $K_v1.4$ and $K_v3.1$ (Fig. 8).

Immunocytochemistry

$K_v1.3$ and $K_v3.1$ proteins were detected with subunit specific antibodies in western blot experiments (Fig. 9a). The predominant bands observed for anti-$K_v1.3$ and anti-$K_v3.1$ antibodies corresponded to proteins with an apparent molecular size of 65 kDa (for the anti-$K_v1.3$ antibody) and 55 kDa (for the anti-$K_v3.1$ antibody), which is similar to the sizes of both K^+ channel subunits deposited in the database ($K_v1.3$ P15384 and $K_v3.1$ P25122). In both cases, these bands disappeared when the antibodies were pre-incubated with their specific antigens. Thus, the detected bands reflected the expression of $K_v1.3$ and $K_v3.1$ proteins. Anti-$K_v1.4$ antibodies failed to detect any protein in these experiments (data not shown).

Immunocytochemical experiments were performed to verify the expression of $K_v1.3$, $K_v1.4$ and $K_v3.1$ channels in the entire population of NPCs. $K_v1.3$ and $K_v3.1$ antibodies stained almost all NPCs which had started to migrate (Fig. 9b–i), whereas $K_v1.4$ antibodies did not stain any NPCs. At higher magnifications, anti-$K_v1.3$ antibodies revealed a staining of cell contours. This points to a partly membrane-associated localization of $K_v1.3$ subunits. A different staining pattern was observed for $K_v3.1$ channels. In this case, the soma of the cells was predominantly stained by anti-$K_v3.1$ antibodies, whereas cellular projections showed almost no fluorescence signal. A pronounced staining of cellular contours could not be observed. The pre-adsorption controls for all used antibodies showed no fluorescence signals. Cells located within the neurosphere were neither accessible for electrophysiological nor for reliable immunocytochemical investigations. Therefore, antibodies were used to stain NPC in cryo-fixated neurosphere slices (Figs 9h and i). Because anti-$K_v1.4$ antibodies failed to stain NPCs, only anti-$K_v1.3$ and anti-$K_v3.1$ antibodies were used in these experiments. The staining displayed co-localization of both channel subunits, with nestin showing channel expression also in resting NPCs. However, these cells were equally stained by the K_v-channel-specific antibodies used, as well as by the nestin specific antibodies.

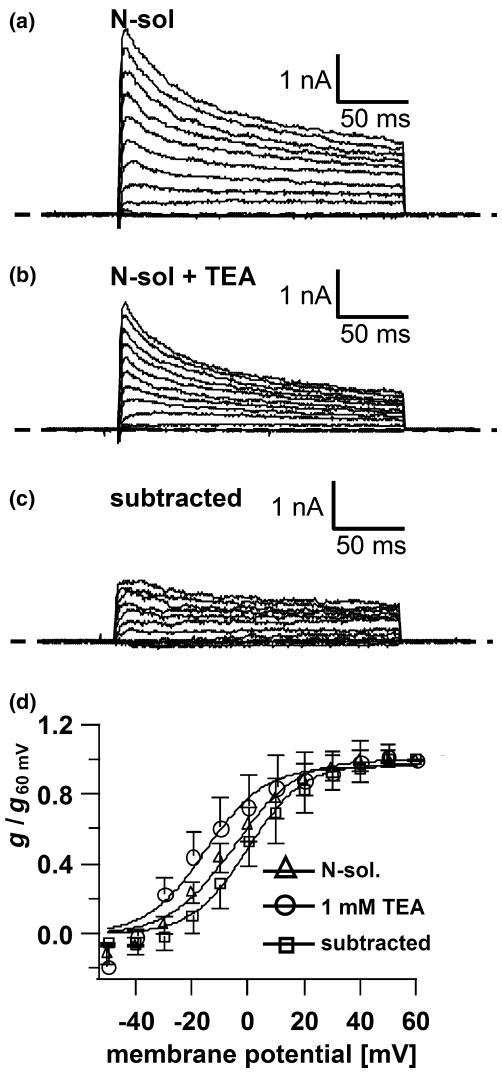

Fig. 5 Voltage dependence. Whole-cell currents were elicited by 200-ms voltage steps from −50 mV to +80 mV with a 10-mV increment. The membrane potential was kept at −80 mV for 10 s between voltage steps. (a) Representative whole-cell currents are shown with N-sol as extracellular solution and (b) N-sol containing 1 mM TEA. These whole-cell currents represent the less TEA-sensitive currents. (c) The highly TEA-sensitive currents were calculated by subtracting whole-cell currents obtained in the presence of 1 mM TEA from currents measured in N-sol. without TEA. (d) Relative whole-cell peak conductance were calculated according to $g/g_{60\ mV}$ with g as the peak conductance and $g_{60\ mV}$ as the peak conductance at +60 mV and plotted against the membrane potential. N-sol assigns data points obtained from experiments with N-sol and 1 mM TEA assigns data points with N-sol containing 1 mM TEA. The currents obtained in N-sol and N-sol + 1 mM TEA were subtracted from each other in order to obtain whole-cell conductances, which correspond to the TEA-sensitive current. Data points for these currents are assigned as subtracted. The curves through the data points were calculated as best fits according to a single Boltzmann equation (for curves through data points, which correspond to currents obtained in N-sol + 1 mM TEA and to the subtracted currents). The curve through data points which corresponds to whole-cell conductances obtained in N-sol without TEA was calculated as best fit according to a double Boltzmann equation.

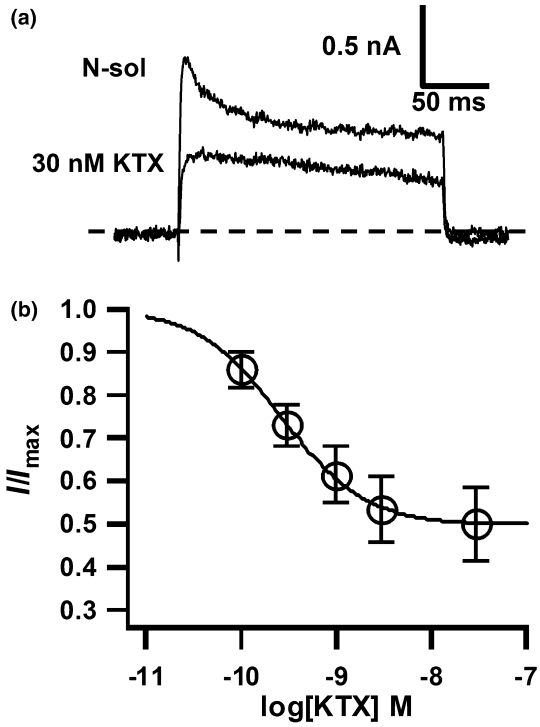

Fig. 6 Effect of Kaliotoxin (KTX) onto whole-cell currents. The membrane potential was stepped from −80 mV to +40 mV for 200 ms and was kept at −80 mV for 30 s between voltage steps. N-sol was used as bath solution. KTX was added to the bath solution in increasing concentrations of 0.1, 0.3, 1, 3 and 30 nM. (a) Representative whole-cell currents are shown. For better clarity, only whole-cell currents with N-sol without any further compound (N-sol) as bath solution and N-sol containing 30 nM KTX (KTX) were shown. (b) Relative peak currents were calculated according to I/I_{max} with I as peak currents measured with N-sol with KTX and I_{max} as peak current measured in N-sol without KTX and were plotted against the KTX concentration. The concentration–response curve through the data points was calculated as best fit according to $I/I_{max} = a_0 + (1-a_0)/(1 + 10\text{^}(\log[KTX]-\log IC_{50}) \times h)$ with I/I_{max} as the relative peak current, a_0 as the relative KTX-insensitive peak current and h as Hill coefficient, which was fixed to $h = 1$. The best fit was obtained for $\log IC_{50} = -9.6 \pm 0.02$ (corresponding to an $IC_{50} = 0.25$ nM) and $a_0 = 0.5 \pm 0.005$.

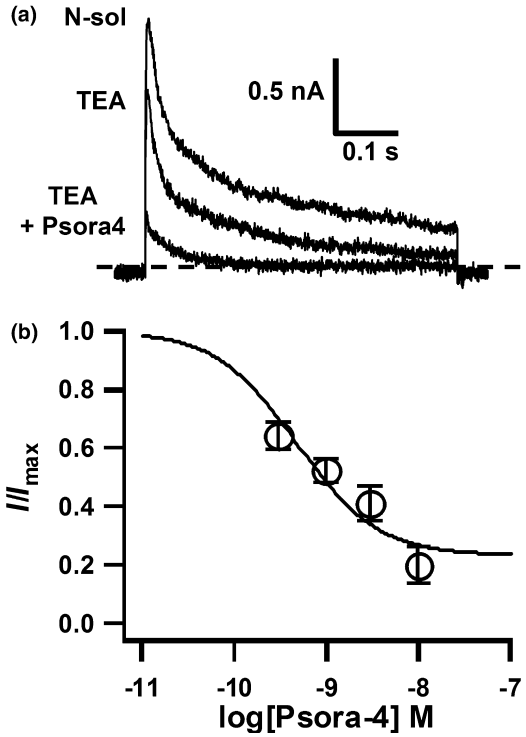

Fig. 7 Effect of Psora-4 on whole-cell currents. The membrane potential was stepped from −80 mV to +40 mV for 500 ms and was kept at −80 mV for 30 s between voltage steps. N-sol without (N-sol) and with 1 mM TEA (TEA) was used as extracellular solution. Psora-4 was added in increasing concentrations of 0.3, 1, 3 and 10 nM to N-sol containing 1 mM TEA. (a) Representative whole-cell currents were shown. For better clarity, only currents in N-sol (N-sol), N-sol + 1 mM TEA (TEA) and N-sol + 1 mM TEA + 10 nM Psora-4 (TEA + Psora4) were shown. (b) Relative peak currents were calculated according to I/I_{max}, with I as peak currents in N-sol containing 1 mM TEA and Psora-4 and I_{max} as peak currents measured in N-sol containing only 1 mM TEA and plotted against the Psora-4 concentration. The concentration–response curve was calculated through the data points as best fit according to $I/I_{1\ mM\ TEA} = a_0 + (1-a_0)/(1 + 10\text{^}(\log[\text{Psora-4}] \times \log IC_{50}) \times h)$ with $I/I_{1\ mM\ TEA}$ as relative peak currents normalized to the peak current measured in the presence of 1 mM TEA, a_0 as the relative TEA- and Psora-4-insensitive peak current and h as the Hill coefficient, which was fixed to $h = 1$. Best fit was obtained for $\log IC_{50} = -9.3 \pm 0.2$ (corresponding to an $IC_{50} = 0.5$ nM and $a_0 = 0.23 \pm 0.07$.

Proliferation assay

Recent studies showed that the blockage of K^+ channels, especially IK and Kv1.3 channels lead to a reduction of cell propagation (Kotecha and Schlichter 1999; Beeton *et al.* 2001). Therefore, we tested whether a selective blockage of the detected K^+ channels can effect NPC proliferation. The incorporation of BrDU-labelled DNA precursors was used to detect currently dividing NPCs via immunofluorescence (Fig. 10). Altogether, 36 neurospheres from three independent isolations were investigated. The number of investigated cells ranged from 300 to 1400 cells per data point. In these experiments, we observed 11 ± 1% (mean ± SEM, $n = 8$) dividing cells within the population of mesencephalic NPCs which were grown under control conditions. The application of 0.01 mM TEA as well as 1 mM tetra-methyl-ammonium ions (TMA) had no effect on NPC growth parameters (Fig. 10c). TEA at low concentrations, as well as its methyl analogue TMA, is known to have no effect on K^+ channels. Thus, these control experiments excluded unspecific side-effects of TEA onto NPCs proliferation. An increase in NPC proliferation rate, however, was obtained by the selective blockage of $K_v3.1$ channels by 1 mM TEA (24 ± 2%, mean ± SEM, $n = 8$) and $K_v1.3$ channels by 10 nM Psora-4 (28 ± 1%, mean ± SEM, $n = 7$). In both cases, the

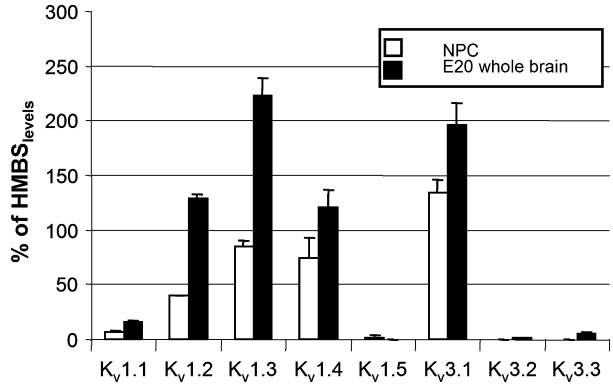

Fig. 8 Semiquantitative real-time RT-PCR on total RNA from undifferentiated NPCs (open bars) and embryonic whole brain at stage E20 (filled bars). Expression levels are shown relative to the housekeeping gene HMBS (mean ± SEM, $n = 4$). Primers and melting curve analysis are given in Fig. 1.

observed increase in proliferation meets the criteria significance (two-tailed unpaired Student's *t*-test; $p = 0.0001$, for 1 mM TEA vs. control and $p = 1e\text{-}7$ for 10 nM Psora-4 vs. control). The combined application of both compounds led to an additional increase of the proliferation rate (31 ± 2%, mean ± SEM, $n = 7$). The additional increase was found to be significant when compared with the proliferation in 1 mM TEA (two-tailed unpaired Student's *t*-test; $p = 0.048$), but not when compared with the proliferation observed with an application of 10 nM Psora-4 alone (two-tailed unpaired Student's *t*-test; $p = 0.27$). These results implicate that the selective blockage of $K_v1.3$ and $K_v3.1$ channels increased NPC proliferation.

Discussion

The regulation of cell proliferation of NPCs is thought to play a key role in regenerative processes in the CNS. There is evidence that ion channels are involved in regulating cell proliferation in a broad variety of cell types, even in different types of progenitor cells. In order to address the question of whether NPCs progeny is also regulated by ion channels, we investigated the functional expression of ion channels in long-term cultured mesencephalic NPCs. The electrophysiological investigations led to the identification of a highly TEA-sensitive K^+ current, which activated at more positive membrane potentials and did not inactivate upon depolarization, resembling the functional properties of $K_v3.1$, but also the properties of $K_v3.2$ and $K_v3.3$ channels. The

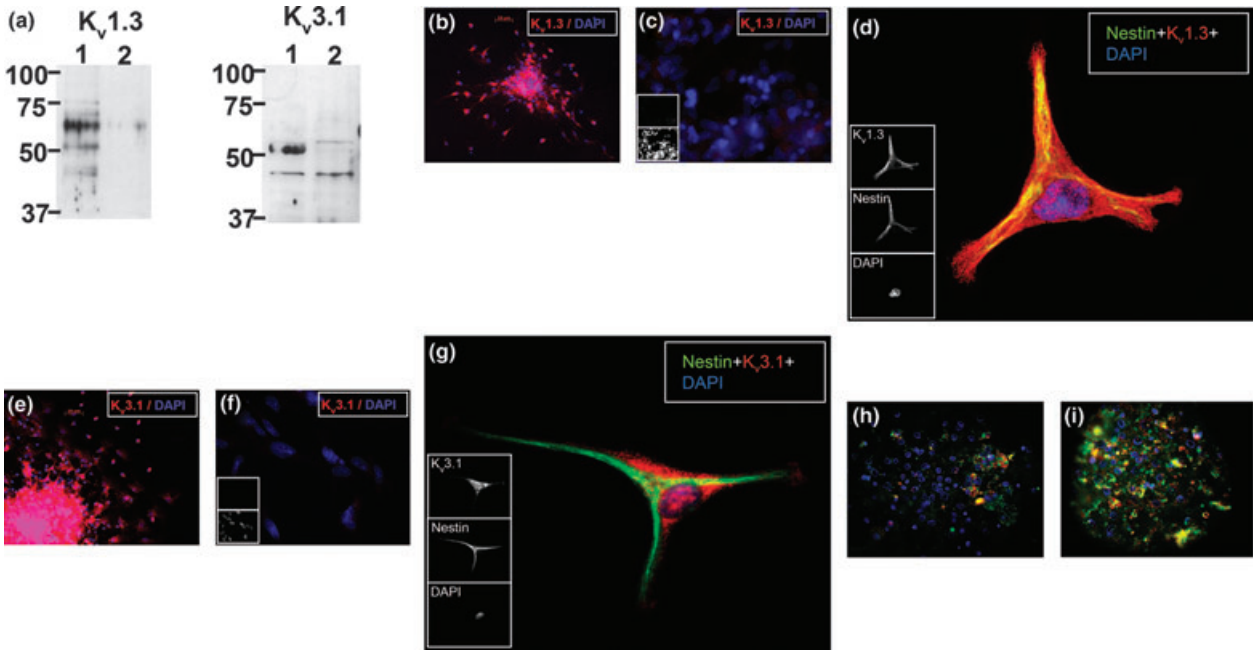

Fig. 9 Immunocytochemical identification of $K_v1.3$ and $K_v3.1$ proteins. (a) Western blots of whole-cell protein extracts from NPC. $K_v1.3$- and $K_v3.1$-specific antibodies were used for immune detection without pre-incubation (lanes 1) and with antigen pre-incubation (lanes 2). Immunocytochemical detection of $K_v1.3$ (b–d) and $K_v3.1$ (e–g) subunits in undifferentiated NPCs. Nuclei were stained by DAPI (blue). Secondary detection was carried out using Alexa 555 (red)- and Alexa 488 (green)-conjugated antibodies. (b) Overview of the whole neurosphere stained for Kv1.3 channels. (magnification 10 x). (c) Pre-adsorption control. (d) Double staining for $K_v1.3$ and nestin proteins. (magnification 63 x). (e) Overview of whole neurosphere stained for $K_v3.1$ channels. (magnification 10 x). (f) Pre-adsorption control. (g) Double staining for $K_v3.1$ and nestin proteins (magnification 63 x). (h) Cryosection stained with anti-$K_v1.3$ (red)/anti-nestin (green) antibodies/DAPI (blue). (i) Cryosection stained with anti-$K_v3.1$ (red)/anti-nestin (green) antibodies/DAPI (blue).

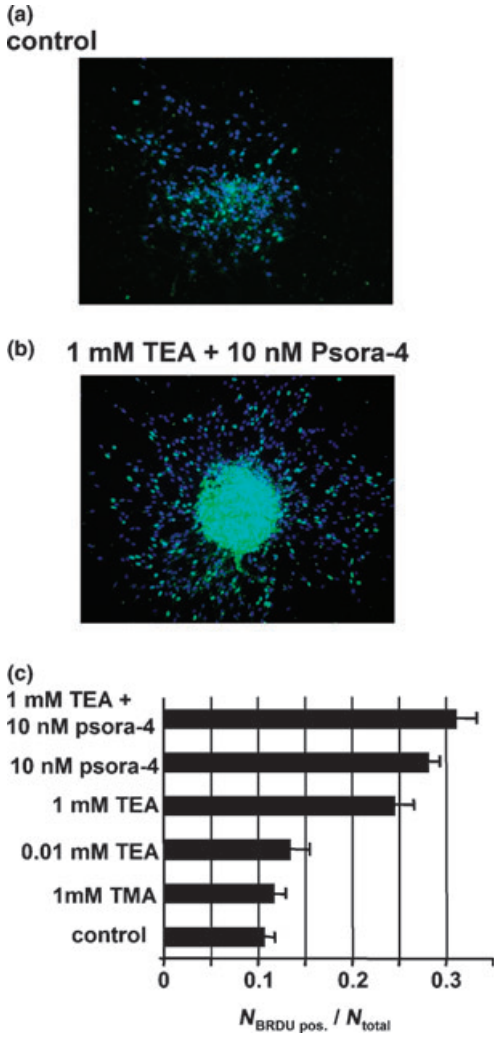

Fig. 10 Proliferation of NPC. Currently dividing cells were identified by immune detection of incorporated BRDU (green). Nuclei were counter stained with DAPI (blue). (a) NPCs cultured under control conditions. (b) NPCs cultured with 1 mM TEA + 10 nM Psora-4. (c) Fractions of dividing cells (calculated as $N_{BRDU\ pos}/N_{total}$ with $N_{BRDU\ pos}$ as number of BrDU-positive cells and N_{total} as number of total cells) under control conditions (control) and in the presence of 1 mM TMA, 0.01 and 1 mM TEA, 10 nM Psora-4 and 1 mM TEA + 10 nM Psora-4.

expression of $K_v3.4$ channels can be excluded, as these K^+ channels are known to exhibit an N-type inactivation (Rettig *et al*. 1992). A second K^+ current component showed an intermediate TEA sensitivity, activated at more negative membrane potentials, and was highly sensitive to Psora-4. There is good evidence that the *Shaker*-like K^+ channel $K_v1.3$ was responsible for this current as KTX partially blocked whole-cell K^+ currents with a subnanomolar potency. The use-dependent reduction of whole-cell currents and the slow time-dependent inactivation resembles typical properties of $K_v1.3$ channels. The K^+-dependent reduction of the major part of the time-dependent inactivating current component suggests an additional K^+ current. A possible explanation for this observation might be the functional expression of $K_v1.4$ channels. This would also explain the TEA and Psora-4 insensitive currents.

The results of the electrophysiological experiments were supported by semiquantitative real-time RT-PCR experiments (Fig. 8) on total RNA from undifferentiated NPCs. The highest RNA levels in NPCs were observed for $K_v1.3$, $K_v1.4$ and $K_v3.1$. These results confirm the electrophysiological experiments. Transcripts for $K_v1.1$ and $K_v1.2$ were detected at reasonable levels by RT-PCR experiments, but there was no evidence for their functional expression from the electrophysiological experiments. This incoherence of transcription and functional expression was observed for $K_v1.1$ and $K_v1.2$, pointing to a possible complex regulation of K^+ channel activity as recently reported (Attali *et al*. 1997; Schmidt *et al*. 1999). However, the transcript levels for both channels were found to be significantly lower than for functionally expressed K^+ channels. The lowest expression levels in NPCs were detected for $K_v1.5$, $K_v3.2$ and $K_v3.3$ transcripts. Therefore, the expression of these channels was excluded, even although the TEA-sensitive current component observed in the electrophysiological investigations gave evidence for their possible expression.

Immunocytochemical experiments were performed in order to investigate the distribution of $K_v1.3$ and $K_v3.1$ subunits in NPC populations. The fact that nearly all migrating NPCs were stained with both antibodies indicates an almost homogenous cell population concerning the expression of $K_v1.3$ and $K_v3.1$ subunits. It also strengthens the conclusion that long-term cultured NPCs co-express subunits of both channels. In mature neurons, $K_v1.3$ are reported to be preferentially targeted to axonal projections (Rivera *et al*. 2005). The observed equal staining of NPCs by anti-$K_v1.3$ antibodies therefore underlines the lack of any cellular polarization in the investigated cells. Contrary to $K_v1.3$ channels, $K_v3.1$ subunits were observed to be predominantly located at the soma of NPCs. This subcellular distribution agrees with the reported localization of these $K_v3.1$ channels to the soma, axonal hillock and axonal compartments of many types of CNS cells (Sekirnjak *et al*. 1997). Anti-$K_v1.4$ antibodies failed to stain NPCs even although the electrophysiological and RT-PCR experiments gave evidence for $K_v1.4$ expression. This observation might be explained by a protein expression level which lies beneath the detection level of the antibody. Cells located within the attached neurospheres showed the co-localization of the stem-cell marker protein nestin with both channel subunits. Thus indicating that the $K_v1.3$ and $K_v3.1$ expression is not restricted to migrating or activated NPCs, but also appears in resting progenitor cells. However, cells located within the neurosphere were unequally stained by both K^+ channel-specific antibodies, as well as by the nestin-specific antibody. This unequal staining might be as a result of variable cutting

layers through NPCs in the neurosphere as well as heterogeneity of cells.

The selective blockage of Kv1.3 and Kv3.1 channels resulted in an increase of NPC proliferation. This observation is in contrast to previous studies, in which the selective blockage of K^+ channels led to an opposite effect, the decrease of cell proliferation (Beeton *et al*. 2001; Jager *et al*. 2004; Beeton *et al*. 2005). It was thought that the hyperpolarizing effect of K^+ channels on the plasma membrane provided a driving force for Ca^{2+} influx into the cytoplasm via Ca^{2+} permeable channels. The resulting increase of the intracellular Ca^{2+} ($[Ca^{2+}]_i$) was believed to trigger cell proliferation. We demonstrated that the selective blockage of K^+ channels had a positive effect on NPC proliferation, which seems to contradict the existing model. There are two main explanations. First, there might be a different or additional mechanism in NPCs regulating the cell cycle, which is independent from a Ca^{2+} influx. Second, the depolarizing effect of the K^+ channel block could lead to a higher open probability of voltage-gated Ca^{2+} channels in NPCs. As the blockage of K^+ channels does not necessarily lead to a shift of the membrane potentials towards the equilibrium potential of Ca^{2+}, the remaining membrane potential could provide a sufficient driving force for an increase of the $[Ca^{2+}]_i$ via a Ca^{2+} influx.

In addition, Zhang *et al*. (2001) described an increase of NPC proliferation under ischaemic conditions associated with elevated levels of EGF. As an EGF-mediated inhibition of the *Shaker*-type $K_v1.2$ and $K_v1.3$ channels (Bowlby *et al*. 1997; Tsai *et al*. 1997; Qiu *et al*. 2003) was recently shown, our study supports the hypothesis that the reported enhancement of NPC proliferation is dependent on $K_v1.3$ inhibition.

NPCs are expected to be utilized as an endogenous source of regenerative cells in the treatment of neurodegenerative processes and tissue damage, e.g. after hypoxia. Proliferation of stem cells *in vitro* and *in vivo* with conserved plasticity is therefore one of the major designations in this experimental field (Hermann *et al*. 2004b). The selective modulation of ion channels like $K_v1.3$ channels by therapeutic usable compounds, such as psoralene derivatives (Vennekamp *et al*. 2004), might provide a more effective way to grow and proliferate NPCs that are to be used for the treatment of neurodegenerative disorders or regeneration of the CNS after, for example, hypoxia.

Acknowledgements

We thank Eberhard Schmid and Paul Walther from the Central Electron Microscopy Unit, University of Ulm for help with high-pressure freezing and LR-gold embedding. This work was supported by the following grants: DFG (Gr 8488–2 to SG), 4SC (Martinsried Germany to SG), Medizinische Fakultät (University of Ulm, P770 to OW and P868 to SL).

References

Attali B., Wang N., Kolot A., Sobko A., Cherepanov V. and Soliven B. (1997) Characterization of delayed rectifier K_v channels in oligodendrocytes and progenitor cells. *J. Neurosci.* **17**, 8234–8245.

Beeton C., Wulff H., Barbaria J., Clot-Faybesse O., Pennington M., Bernard D., Cahalan M. D., Chandy K. G. and Beraud E. (2001) Selective blockade of T lymphocyte K^+ channels ameliorates experimental autoimmune encephalomyelitis, a model for multiple sclerosis. *Proc. Natl Acad. Sci. USA* **98**, 13 942–13 947.

Beeton C., Pennington M. W., Wulff H. *et al.* (2005) Targeting effector memory T cells with a selective peptide inhibitor of $K_v1.3$ channels for therapy of autoimmune diseases. *Mol. Pharmacol.* **67**, 1369–1381.

Bowlby M. R., Fadool D. A., Holmes T. C. and Levitan I. B. (1997) Modulation of the $K_v1.3$ potassium channel by receptor tyrosine kinases. *J. Gen. Physiol.* **110**, 601–610.

Gallo V., Zhou J. M., McBain C. J., Wright P., Knutson P. L. and Armstrong R. C. (1996) Oligodendrocyte progenitor cell proliferation and lineage progression are regulated by glutamate receptor-mediated K^+ channel block. *J. Neurosci.* **16**, 2659–2670.

Gomez-Hernandez J. M., Lorra C., Pardo L. A., Stuhmer W., Pongs O., Heinemann S. H. and Elliott A. A. (1997) Molecular basis for different pore properties of potassium channels from the rat brain K_v1 gene family. *Pflugers Arch.* **434**, 661–668.

Grissmer S., Nguyen A. N., Aiyar J., Hanson D. C., Mather R. J., Gutman G. A., Karmilowicz M. J., Auperin D. D. and Chandy K. G. (1994) Pharmacological characterization of five cloned voltage-gated K^+ channels, types $K_v1.1$, 1.2, 1.3, 1.5, and 3.1, stably expressed in mammalian cell lines. *Mol. Pharmacol.* **45**, 1227–1234.

Herberth B., Pataki A., Jelitai M., Schlett K., Deak F., Spat A. and Madarasz E. (2002) Changes of KCl sensitivity of proliferating neural progenitors during *in vitro* neurogenesis. *J. Neurosci. Res.* **67**, 574–582.

Hermann A., Gastl R., Liebau S. *et al.* (2004a) Efficient generation of neural stem cell-like cells from adult human bone marrow stromal cells. *J. Cell Sci.* **117**, 4411–4422.

Hermann A., Gerlach M., Schwarz J. and Storch A. (2004b) Neurorestoration in Parkinson's disease by cell replacement and endogenous regeneration. *Expert Opin. Biol. Ther.* **4**, 131–143.

Jager H., Dreker T., Buck A., Giehl K., Gress T. and Grissmer S. (2004) Blockage of intermediate-conductance Ca^{2+}-activated K^+ channels inhibit human pancreatic cancer cell growth *in vitro*. *Mol. Pharmacol.* **65**, 630–638.

Knutson P., Ghiani C. A., Zhou J. M., Gallo V. and McBain C. J. (1997) K^+ channel expression and cell proliferation are regulated by intracellular sodium and membrane depolarization in oligodendrocyte progenitor cells. *J. Neurosci.* **17**, 2669–2682.

Kotecha S. A. and Schlichter L. C. (1999) A $K_v1.5$ to $K_v1.3$ switch in endogenous hippocampal microglia and a role in proliferation. *J. Neurosci.* **19**, 10 680–10 693.

Legros C., Pollmann V., Knaus H. G., Farrell A. M., Darbon H., Bougis P. E., Martin-Eauclaire M. F. and Pongs O. (2000) Generating a high-affinity scorpion toxin receptor in $K_{cs}A$-$K_v1.3$ chimeric potassium channels. *J. Biol. Chem.* **275**, 16 918–16 924.

Motulsky H. and Christopoulos A. (2004) Fitting dose–response curves, in *Fitting Models to Biological Data Using Linear and Non-Linear Regression: A Practical Guide to Curve Fitting* (Motulsky H. and Christopoulos A., eds), pp. 256–295. Oxford University Press, New York.

Qiu M. H., Zhang R. and Sun F. Y. (2003) Enhancement of ischemia-induced tyrosine phosphorylation of $K_v1.2$ by vascular endothelial

growth factor via activation of phosphatidylinositol 3-kinase. *J. Neurochem.* **87**, 1509–1517.

Rettig J., Wunder F., Stocker M. *et al.* (1992) Characterization of a Shaw-related potassium channel family in rat brain. *EMBO J.* **11**, 2473–2486.

Ribera A. B. (1999) Potassium currents in developing neurons. *Ann. NY Acad. Sci.* **868**, 399–405.

Rivera J. F., Chu P. J. and Arnold D. B. (2005) The T1 domain of $K_v1.3$ mediates intracellular targeting to axons. *Eur. J. Neurosci.* **22**, 1853–1862.

Schmidt K., Eulitz D., Veh R. W., Kettenmann H. and Kirchhoff F. (1999) Heterogeneous expression of voltage-gated potassium channels of the shaker family (K_v1) in oligodendrocyte progenitors. *Brain Res.* **843**, 145–160.

Sekirnjak C., Martone M. E., Weiser M., Deerinck T., Bueno E., Rudy B. and Ellisman M. (1997) Subcellular localization of the K^+ channel subunit $K_v3.1b$ in selected rat CNS neurons. *Brain Res.* **766**, 173–187.

Spitzer N. C., Vincent A. and Lautermilch N. J. (2000) Differentiation of electrical excitability in motoneurons. *Brain Res. Bull.* **53**, 547–552.

Storch A., Paul G., Csete M., Boehm B. O., Carvey P. M., Kupsch A. and Schwarz J. (2001) Long-term proliferation and dopaminergic differentiation of human mesencephalic neural precursor cells. *Exp. Neurol.* **170**, 317–325.

Tsai W., Morielli A. D. and Peralta E. G. (1997) The m1 muscarinic acetylcholine receptor transactivates the EGF receptor to modulate ion channel activity. *EMBO J.* **16**, 4597–4605.

Vautier F., Belachew S., Chittajallu R. and Gallo V. (2004) Shaker-type potassium channel subunits differentially control oligodendrocyte progenitor proliferation. *Glia* **48**, 337–345.

Vega-Saenz d. M., Moreno H., Fruhling D., Kentros C. and Rudy B. (1992) Cloning of ShIII (Shaw-like) cDNAs encoding a novel high-voltage-activating, TEA-sensitive, type-A K^+ channel. *Proc. Biol. Sci.* **248**, 9–18.

Vennekamp J., Wulff H., Beeton C., Calabresi P. A., Grissmer S., Hansel W. and Chandy K. G. (2004) $K_v1.3$-blocking 5-phenylalkoxypsoralens: a new class of immunomodulators. *Mol. Pharmacol.* **65**, 1364–1374.

Walther P. and Ziegler A. (2002) Freeze substitution of high-pressure frozen samples: the visibility of biological membranes is improved when the substitution medium contains water. *J. Microsc.* **208**, 3–10.

Wang D. D., Krueger D. D. and Bordey A. (2003) Biophysical properties and ionic signature of neuronal progenitors of the postnatal subventricular zone *in situ*. *J. Neurophysiol.* **90**, 2291–2302.

Zhang R. L., Zhang Z. G., Zhang L. and Chopp M. (2001) Proliferation and differentiation of progenitor cells in the cortex and the subventricular zone in the adult rat after focal cerebral ischemia. *Neuroscience* **105**, 33–41.

